Sub-surface metrology using scanning white light interferometry: absolute z-coordinates deep inside displays

ANTON NOLVI,[1,*] IVAN KASSAMAKOV,[1] EDWARD HÆGGSTRÖM[1]

[1]Department of Physics, University of Helsinki, P.O. 64, 00014 FINLAND
*Corresponding author: anton.nolvi@helsinki.fi

Received XX Month XXXX; revised XX Month, XXXX; accepted XX Month XXXX; posted XX Month XXXX (Doc. ID XXXXX); published XX Month XXXX

Mobile devices with interactive displays are ubiquitous commodities. Efficient quality control (QC) drives competitiveness. Scanning White Light Interferometry (SWLI) imaging offers a fast and non-destructive tool for QC purposes. Relying on optical compensation and image stitching one can rapidly and cost-effectively produce sharp 3D-images of a display's inner structures with a few nanometers accuracy along the z-direction. As a practical example 3D images of a mobile device display revealed 0.92±0.02 µm height variation in the top glass assembly. The proposed method improves quality assurance methods of display manufacturing.

OCIS codes: *(120.0120) Instrumentation, measurement, and metrology; (120.3180) Interferometry; (100.3175) Interferometric imaging.*

http://dx.doi.org/00.0000/AO.00.000000

1. INTRODUCTION

Mobile devices, e.g. smartphones and handheld multi-use tablets with interactive displays are common. Competition is intense and a product has to be innovative and offer quality at low price. Quality is built into the product by engineering and effective quality control. In these devices the quality of the display, the touch-screen interface, is important since it affects user experience.

The display is a stack of multiple layers [1, 2]. From a quality point of view, the air gap distance between the glass plate and the display pixel base is important [1], Fig. 1. The glass is attached to the base with an adhesive that runs along its edges and that determines the air gap [3]. An uneven adhesive thickness may generate stress into the glass which reduces the durability of the display. In addition, any tilt between the base and glass reduces the optical properties of the display.

Current imaging methods which are suitable for assuring the air gap related quality of displays rely on 2D cameras which monitor only the pre-assembly application of adhesive [4, 5]. Post-assembly structural imaging requires sample preparation [4] which reduces production yield. Moreover, destructive sample preparation may affect the sample and bias the quality reading.

SWLI offers a non-destructive imaging method that requires no sample preparation. It produces a fast and cost-effective manner sharp 3D-images with a few nanometers vertical resolution that are suitable for quality control of displays. The SWLI technology is gaining popularity in metrology [6-8].

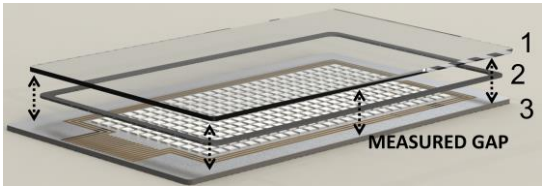

Fig. 1. Exploded view of simplified display structure showing relevant layers: 1. top glass plate, 2. adhesive, 3. main base (pixels, electronics etc.). Arrows indicate the measured gap between main base floor and inner surface of top glass.

2. METHODS

A. Scanning White Light Interferometry

SWLI has progressed from imaging a sample's accessible top surface to 3D through-layer imaging of buried features [9] and to dynamic measurements of rapidly oscillating structures [10]. There are efforts to bring traceability into static and dynamic SWLI-based measurements [11].

An optical interferometer based on SWLI relies on the broad spectrum of its light source and allows imaging with high vertical resolution. The interferometer, typically featuring a compact interferometric objective, comprises one fixed reference mirror path and one variable light path that reflects off the sample, Fig. 2. When altering the path to the sample by scanning the objective through a certain range, interference fringes appear. Measuring the light intensity in relation to the objective-sample distance, interference data which

describes the sample are obtained. From this data, the sample's distance from the objective can be precisely calculated [12-14].

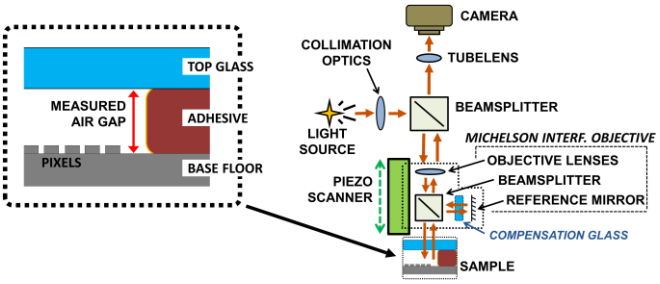

Fig. 2. Schematic of measured structure and interferometer device.

B. LAYER COMPENSATION TECHNIQUE

In addition to accessible single surface sample imaging, SWLI can be used also to image through optically clear layers. However, the layer thickness through which internal features of a sample can be imaged is limited since the layer offsets the interference fringe plane from the shifted objective's focal plane [15], Fig. 3.

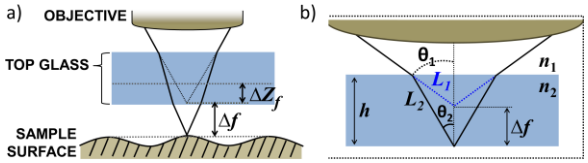

Fig. 3. (a) Focal plane shift (Δf) and interference fringe plane shift (Z_f) when imaging through a thick top glass, (b) ray geometry *(incident angles θ)* resulting in optical path (L) differences due to glass *(thickness h, refractive index n_2).*

When imaging with objective (numerical aperture $NA = n_1 \sin\theta_1$, where n_1 is the refractive index of object space and θ_1 is the half angle of the objective's collecting cone) through a glass layer (refractive index n_2, thickness h) the shift of the focal plane (Δf) can be expressed as [16]

$$\Delta f = h\frac{\sqrt{{n_1}^2-NA^2}}{\sqrt{{n_2}^2-NA^2}}. \quad (2)$$

Similarly interference plane shift (ΔZ_f) can be expressed as

$$\Delta Z_f = n_2 L_2 - n_1 L_1 = h\left(\frac{n_2}{\sqrt{{n_2}^2-NA^2}} - \frac{n_1}{\sqrt{{n_1}^2-NA^2}}\right). \quad (1)$$

Here an approximation of using similar refractive indexes in both equations (1) and (2) is used.

With thin layers and especially with objectives having low NA, the offset fits into the depth of focus. When the layer thickness increases, the interference plane shifts outside the depth of focus. This larger offset needs to be corrected for if undistorted mapping of internal structures is desired. For a thick top layer, e.g. the cover glass of a display, a compensating material with similar optical properties (thickness and refractive index) can be put in the reference arm of the interferometer. This brings the interference fringes back onto objective's focus plane and makes the fringes sharp to the camera. Using this compensation technique, detailed scans can be obtained even through thick layers.

With low NA objectives, their large depth of focus allows freedom when selecting a compensation glass. It is preferable, but not mandatory, to use the exact same kind of glass as compensation plate and as top glass. This is to ensure the same optical path, but additional dispersion effects must also be accounted for.

C. STITCHING

The lateral dimensions of a single scan are limited by the optical magnification and by the camera sensor size. If high spatial resolution across an object larger than area covered by single scan image is desired, a stitching method can be applied. In this method the imaged object is divided into many high magnification scans and by post-processing algorithms combined into a single large area scan image.

The uncertainty in translation between sub-image scans introduces artifacts into the compounded image, Fig. 4. These uncertainties are reduced by stitching algorithms based on calculations between overlapping (> 20%) parts of adjacent images [17]. For simple relatively flat 3D surfaces, as in this particular case, methods based on the Otsubo, Okada, and Tsujiuchi [18] are sufficient and commonly used. More complex multiple curved surfaces can be stitched using methods proposed by Sjödahl and Oreb [19].

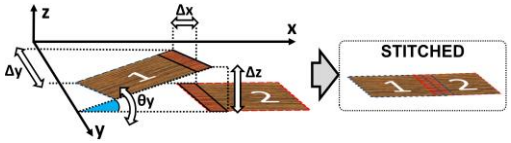

Fig. 4. Shifting and tilting (thick arrows) of two adjacent images due to translation uncertainty. Shaded regions present the overlapping part that the stitching algorithm exploits. Shifting and tilting occur in relation to all axes. For illustrative purposes, only tilt around the y-axis is presented.

D. HARDWARE

The SWLI-based device, Fig. 5a, is built on a reflective light microscope (ASKANIA Mikroskop Technik Rathenow) attached to a custom frame. A halogen lamp (G4 6V 10W, OSRAM) serves as a light source. The image is captured with a CMOS camera (C11440 Orka Flash2.8, HAMAMATSU). The vertical scan (z) is done with a piezo-electric objective scanner (P-721 PIFOC, PI), and the horizontal sample translation (x, y) is realized by two motorized translation stages (8MT167-25LS, STANDA).

The interferometer part is formed with an infinity corrected 5x Michelson-type interferometric objective (CF PLAN 5x/0.13 TI, NIKON, NA 0.13, working distance 9.3 mm). The objective is equipped with a slot for blocking the reference arm path between the beam splitter (B.S.) and the reference mirror. This slot is used to house the compensation glass, Fig. 5b. The objective is coupled with a 0.63x tube lens (ASKANIA Mikroskop Technik Rathenow), for a total magnification of 3.15x and single scan field of view 2.2 x 1.7 mm.

A custom-built software collects and calculates the scanned interferometric data to produce 3D-data of the sample. Commercial software (MountainsMap, DIGITAL SURF) is used for 3D-data analysis (stitching and height profile measurements) for easy industrial applicability to the QC.

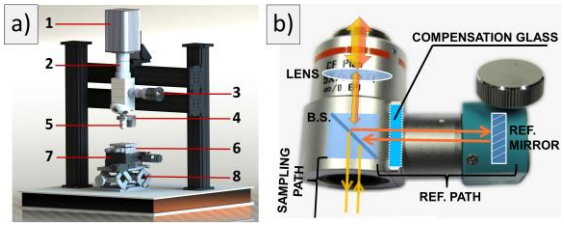

Fig. 5. (a) Device setup: 1-camera, 2-tube lens, 3-light source, 4-piezo-scanner, 5-interferometric objective, 6-tilt-stage, 7-horizontal translation stages and 8-labjack. (b) Michelson interferometric objective with reference arm slot usable as compensation glass holder.

D. VALIDATION

The through-layer measurement accuracy of the device was validated by imaging a layered test sample, Fig. 6., with Scanning Electron Microscope (SEM) (S4800, HITACHI; 10.0 kV, working distance 10.7 mm, 300x). For SEM imaging, the sample was coated with gold (4 nm thick layer) in a sputtering chamber. The sample consisted of two glued glass plates (Borosilicate Glass, Thickness No.1, VWR INTERNATIONAL) stacked to form a gap.

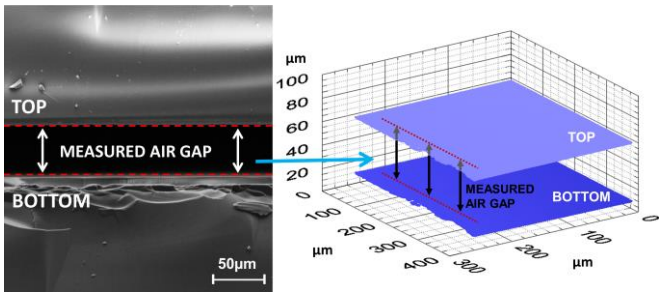

Fig. 6. (Left): Side view SEM image, and (Right): image measured with the interferometer device of the embedded surfaces of the layered test sample. The air gap distance between inner glass plate surfaces (red dotted line) was measured.

The average gap between the inner surfaces of two stacked glasses measured at 10 points along the edge was 47.12±0.15 µm with interferometer and 47.43±0.19 µm with SEM.

E. SAMPLE AND MEASUREMENT PROCEDURE

For QC purposes, a mobile device display was examined to determine the air gap between two of its embedded surfaces (main pixel base floor and inner surface of top glass). The display was imaged "as is" without preparation and the measurement procedure is easily handled even by a non-specialist. The imaging time for single image scan, covering area of 2.2 x 1.7 mm, was few tens of seconds.

Multiple images were obtained from each corner of the display and stitched to produce accurate 3D-scans for analysis. The embedded surface features were imaged through the display's 299±1 µm thick top glass. A compensating glass with similar optical properties (stack of two thickness #1 glass cover slips (Borosilicate glass, No.1, VWR INTERNATIONAL)) was used.

3. RESULTS

Stitched 3D-scans of each corner of the display (5 sub-scans from top-right and 3 from the rest) were measured. Figure 7 shows the 3D images of corners with the measured profile lines indicated as dashed lines. A single center-most profile for each corner (red dashed line) showing the structural dimensions is presented as a graph. The air gap distance between the embedded main base floor and the inner surface of the top glass varied by as much as 0.92±0.02 µm between different regions of display.

The top glass resides on an adhesive lining. Its upper surface of the lining exhibits effectively on the same height coordinate as the surface of top glass. Since the visible surface of the top glass does not bring value to the 3D analysis, it is not shown in the 3D-images.

Profiles every 20 mm along the adhesive line where recorded by circling the display clockwise before, center, and after each corner. Heights from the common base floor level to the raising edge of the adhesive lining represent display's air gap values, Table 1.

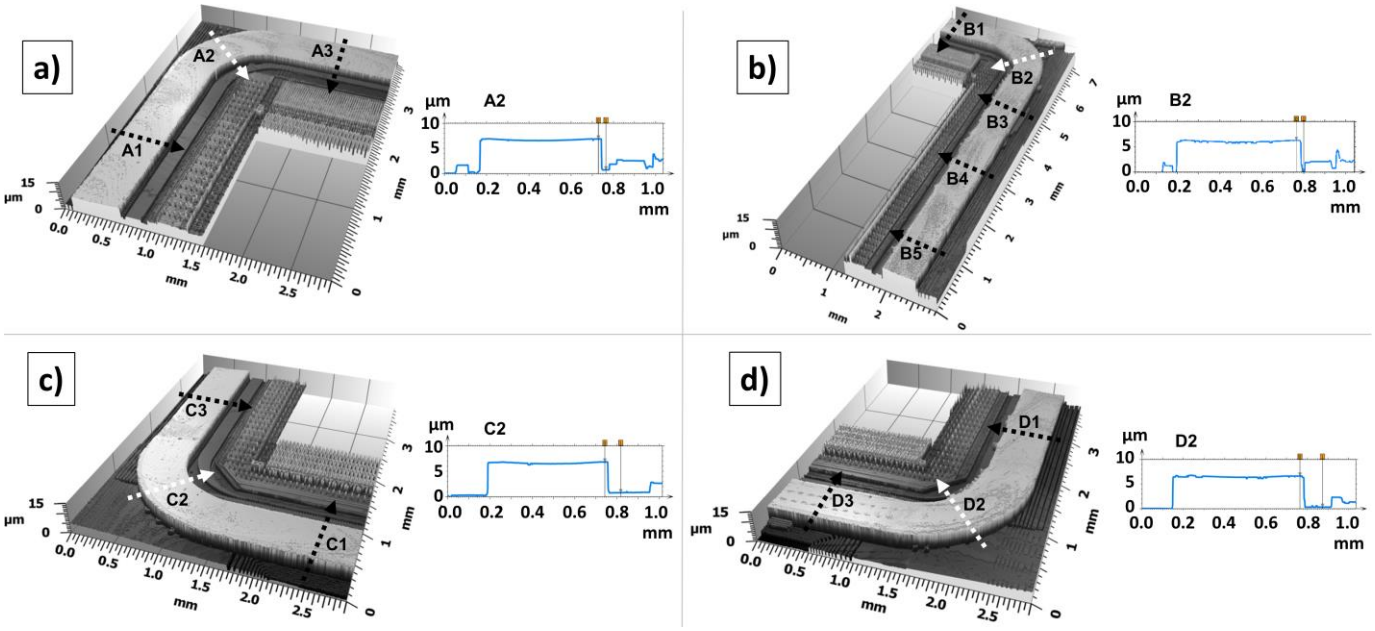

Fig. 7. 3D-scans from corners of a mobile display: (a) Top left, (b) top right, (c) bottom left, and (d) bottom right corner. The red arrows indicate positions of profile lines from each corner showed as a graph next to 3D images.

Table 1. Air gap distances of the measured display.[a]

		Profile lines				
Position		1	2	3	4	5
TOP-LEFT	A	6.25 µm	6.15 µm	5.56 µm		
TOP-RIGHT	B	5.89 µm	6.12 µm	6.21 µm	6.36 µm	6.42 µm
BOTTOM-LEFT	C	6.48 µm	6.04 µm	6.05 µm		
BOTTOM-RIGHT	D	6.36 µm	6.32 µm	6.24 µm		

[a]Uncertainty for each value is ±0,01µmm, as defined in [20].

4. DISCUSSION

Measured 3D-scan images of a mobile device display revealed air gap distance variations between the inner surface of the top glass and the main common pixel base floor. The precise height values were obtained by extracting cross-cut line data from the 3D-images.

Since the images were taken through the protective glass layer without sample preparation, the imaging did not affect the structure and functionality of the displays. Compared to point measurement based methods [21, 22], our method produces in significantly faster way full 3D data from a large area of the sample. From a quality control perspective, this is advantageous. The parameters for quality control of each manufactured product can be examined.

The SWLI-imaging produced sharp 3D overview images with precise internal coordinates well suited for the presented QC purpose. The highly-resolved rich internal structural features seen in the images can provide further data for detailed quality assurance purposes. From this 3D-data, the structural quality of the display can be accurately and quickly determined.

The stitching can generate small artefacts on the stitched 3D data. In reference measurements for the used stitching method, an average of 0.07±0.02 µm increase in the overall surface roughness across entire area was detected. The stitched large overall 3D view is absolutely necessary on determine the common main base floor surface (see Fig. 1) for every individual height profile lines to avoid false base surface identification (e.g. as seen in the Fig. 7a profile A2). By selecting profile lines inside sub-image scans, there is no stitching generated uncertainty to the height measurements.

The SWLI is limited by the optical properties of the imaged sample. The through-imaged layer has to be optically transparent for the camera and light source used. In addition to glass-like visually transparent materials, silicon materials are optically transparent in the infrared region. When using a broadband light source, this can be easily achieved by simply changing the camera to infrared type.

Furthermore, the optical thickness of the through-imaged layer relative to the compensation layer is critical when high measurement accuracy is required. In the display case, the optical thickness of the top glass is constant and easily matched with a compensation layer. Uncompensated large variations in the optical thickness, geometrical thickness or refractive index changes, of through imaged layer would induce artifacts in the image of the embedded structures.

In addition to imaging stationary displays, the presented approach can potentially be applied to imaging oscillating samples covered with glass or silicon.

5. CONCLUSIONS

The ability of SWLI-imaging was presented with stationary through-thick-glass sample imaging. SWLI-imaging offers a non-destructive tool for quality control purposes of mobile device displays. It produces sharp 3D images of their inner structures without sample preparation (high resolution across large areas) in fast and cost-effective manner.

Acknowledgment. We thank M.Sc. Tuomo Ylitalo and Ph.D. Aneliya Karadzhinova for their help.

References

1. J. Chen, W. Cranton and M.Fihn, *Handbook of Visual Display Technology* (Springer, 2012), Chap. 5.7.
2. G. Walker, "A review of technologies for sensing contact location on the surface of a display," Journal of the SID, **20(**8), 413-440 (2012).
3. T. Tsujimura, *OLED displays: Fundamentals and applications (*Wiley, 2012), Chap. 3.
4. J. Schlett, "Machine vision helps adhesive trend stick in auto industry," (Photonics Media, 2016), http://www.photonics.com/Article.aspx?AID=61129.
5. R. Tremblay, "3-D Vision Enables Challenging Adhesive Inspection Applications," (Adhesives & Sealants Industry, 2016), http://www.adhesivesmag.com/articles/94619--d-vision-enables-challenging-adhesive-inspection-applications.
6. Y. Wang, E.I. Meletis and H. Huang, "Quantitative study of surface roughness evolution during low-cycle fatigue of 316L stainless steel using Scanning Whitelight Interferometric (SWLI) Microscopy," Int. J. Fatique **48**, 280-288 (2013).
7. U. Paaver, J. Heinämäki, I. Kassamakov, E. Hæggström, T. Ylitalo, A. Nolvi, J. Kozlova, I. Laidmäe, K. Kogermann and P. Veski, "Nanometer depth resolution in 3D topographic analysis of drug-loaded nanofibrous mats without sample preparation," Int. J. Pharm **462**(1-2), 29-37 (2014).
8. A. Karadzhinova, A. Nolvi, R. Veenhof, E. Tuominen, E. Hæggström and I. Kassamakov, "Impact of GEM foil hole geometry on GEM detector gain,"JINST **10**, P12014 (2015).
9. V. Heikkinen, I. Kassamakov, T. Paulin, A. Nolvi and E. Hæggström, "Stroboscopic scanning white light interferometry at 2.7 MHz with 1.6 µm coherence length using a non-phosphor LED source," Opt. Express **21**, 5247-5254 (2013).
10. A. Nolvi, V. Heikkinen, I. Kassamakov, J. Aaltonen, T. Ylitalo, O. Saresoja, M. Berdova, S. Franssila and E. Hæggström, "IR-SWLI for subsurface imaging of large MEMS structures," Proc. SPIE **8430**, 843018 (2012).
11. V. J. Seppä, I. Kassamakov, A. Nolvi, V. Heikkinen, T. Paulin, A. Lassila, L. Hao, E. Hæggström, "Static and (quasi)dynamic calibration of stroboscopic scanning white light interferometer," Proc. SPIE **8788**, 87883J (2013).
12. J. C. Wyant, "White light interferometry," Proc. SPIE **4737**, 98-107 (2002).
13. K, Larkin, "Efficient nonlinear algorithm for envelope detection in white light interferometry," J. Opt. Soc. Am. A **13**, 832-843 (1996).
14. A, Harasaki, J. Schmit and J.C. Wyatt, "Improved Vertical-Scanning Interferometry," Appl. Optics **39**, 2107-2115 (2000).
15. P. C. Montgomery, D. Benhaddou and D. Montaner, "Interferometric roughness measurement of Ohmic contact/III–V semiconductor interfaces," Appl. Phys. Lett. **71**, 1768-1770 (1997).
16. M. Haruna, M. Ohmi, T. Mitsuyama, H. Tajiri, H. Maruyama, and M. Hashimoto, "Simultaneous measurement of the phase and group indices and the thickness of transparent plates by low-coherence interferometry," Opt. Lett. **23**, 966-968 (1998).

17. J. C. Wyant and J. Schmit, “Large field of view, high spatial resolution, surface measurements,” Int. J. Mach. Tool Manu. **38**(5-6), 691-698 (1998).
18. M. Otsubo, K. Okada and J. Tsujiuchi, “J., “Measurement of large plane surface shapes by connecting small-aperture interferograms,” Opt. Eng. **33**(2), (1994).
19. M. Sjödahl and B. F. Oreb, “Stitching interferometric measurement data for inspection of large optical components,” Opt. Eng. **41**(2), 403-408 (2002).
20. Evaluation of measurement data — Guide to the expression of uncertainty in measurement (GUM), UKAS JCGM 100:2008
21. Z. Xu, V. Shilpiekandula, K. Youcef-Toumi, and S. F. Yoon, “White-light scanning interferometer for absolute nano-scale gap thickness measurement,” Opt. Eng. **17**(17), 15104-15117 (2009).
22. A. Courteville, R. Wilhelm and F. Garcia, "A novel, low coherence fiber optic interferometer for position and thickness measurements with unattained accuracy," Proc. SPIE **6189**, 618918 (2006).